HHS Public Access
Author manuscript
Neurobiol Dis. Author manuscript; available in PMC 2021 April 23.

Published in final edited form as:
Neurobiol Dis. 2021 March ; 150: 105254. doi:10.1016/j.nbd.2021.105254.

Facilitation of GluN2C-containing NMDA receptors in the external globus pallidus increases firing of fast spiking neurons and improves motor function in a hemiparkinsonian mouse model

Jinxu Liu[a,1], **Gajanan P. Shelkar**[a,1], **Lopmudra P. Sarode**[b], **Dinesh Y. Gawande**[a], **Fabao Zhao**[c], **Rasmus Praetorius Clausen**[c], **Rajesh R. Ugale**[b], **Shashank Manohar Dravid**[a,*]

[a]Department of Pharmacology and Neuroscience, Creighton University School of Medicine, Omaha, NE 68178, United States of America

[b]Department of Pharmaceutical Sciences, Rashtrasant Tukadoji Maharaj Nagpur University, Nagpur, Maharashtra 440033, India

[c]Department of Drug Design and Pharmacology, Faculty of Health and Medical Sciences, University of Copenhagen, Universitetsparken 2, 2100 Copenhagen, Denmark

Abstract

Globus pallidus externa (GPe) is a nucleus in the basal ganglia circuitry involved in the control of movement. Recent studies have demonstrated a critical role of GPe cell types in Parkinsonism. Specifically increasing the function of parvalbumin (PV) neurons in the GPe has been found to facilitate motor function in a mouse model of Parkinson's disease (PD). The knowledge of contribution of NMDA receptors to GPe function is limited. Here, we demonstrate that fast spiking neurons in the GPe express NMDA receptor currents sensitive to GluN2C/GluN2D-selective inhibitors and glycine site agonist with higher efficacy at GluN2C-containing receptors. Furthermore, using a novel reporter model, we demonstrate the expression of GluN2C subunits in PV neurons in the GPe which project to subthalamic nuclei. GluN2D subunit was also found to localize to PV neurons in GPe. Ablation of GluN2C subunit does not affect spontaneous firing of fast spiking neurons. In contrast, facilitating the function of GluN2C-containing receptors using glycine-site NMDA receptor agonists, D-cycloserine (DCS) or AICP, increased the spontaneous

*Corresponding author at: Department of Pharmacology and Neuroscience, Creighton University, School of Medicine, 2500 California Plaza, Omaha, NE 68178, United States of America. ShashankDravid@creighton.edu (S.M. Dravid).

[1]Equal contribution.

CRediT authorship contribution statement

Jinxu Liu: Conceptualization, Data curation, Investigation, Formal analysis. **Gajanan P. Shelkar:** Conceptualization, Data curation, Investigation, Formal analysis, Writing - original draft. **Lopmudra P. Sarode:** Conceptualization, Data curation, Investigation, Formal analysis. **Dinesh Y. Gawande:** Conceptualization, Formal analysis. **Fabao Zhao:** Data curation, Investigation. **Rajesh R. Ugale:** Conceptualization, Data curation, Investigation, Formal analysis, Writing - original draft. **Shashank Manohar Dravid:** Conceptualization, Data curation, Investigation, Formal analysis, Writing - original draft

Author contributions

JL, GPS, RRU, SMD conducted experiments, contributed to writing the manuscript and/or analyzed data. FZ and RPC synthesized AICP. All authors contributed to research design and reviewed the final manuscript.

The authors note no conflict of interest.

Supplementary data to this article can be found online at https://doi.org/10.1016/j.nbd.2021.105254.

firing frequency of PV neurons in a GluN2C-dependent manner. Finally, we demonstrate that local infusion of DCS or AICP into the GPe improved motor function in a mouse model of PD. Together, these results demonstrate that GluN2C-containing receptors and potentially GluN2D-containing receptors in the GPe may serve as a therapeutic target for alleviating motor dysfunction in PD and related disorders.

Keywords

NMDA; GluN2C; GRIN2C; Parkinson's disease; Parvalbumin; Oscillations

1. Introduction

Globus pallidus externa (GPe) is a nucleus in the basal ganglia circuitry that constitutes part of the indirect pathway and serves as a relay station between striatum and the subthalamic nuclei (STN). The GPe is composed primarily of GABAergic neurons except for ~5% of choline acetyl transferase (ChAT)-positive neurons. Originally two cell types based on the firing pattern were discovered known as high frequency pausers (Type I) and low frequency bursters (Type II) (DeLong, 1971). Recently, using genetic reporter lines a more comprehensive classification of GPe cell types has been established which include; parvalbumin (PV) expressing cells that closely corresponds to the Type I cells and exhibit fast and regular bursting. The PV neurons project strongly to the STN and also to parafascicular thalamus; and Npas1^{+} cells which resemble the Type II cells and have slow and irregular bursting (Hernandez et al., 2015). Another classification based upon a separate set of markers is into; PV, arkypallidal and Lhx6 cells. The arkypallidal cells express preproenkephalin and project to the striatal spiny neurons and interneurons (Mallet et al., 2012). On the other hand the Lhx6 neurons project to STN and SNc as well as to fast-spiking neurons in the striatum (Mastro et al., 2014; Abdi et al., 2015). Due to the differences in the output of the different cell classes, it is conceivable that selective targeting of cell-types can yield desirable effects on the indirect pathway and the overall basal ganglia pathway.

The knowledge of the contribution of NMDA receptors to the physiology of GPe neurons is limited. Local inhibition of NMDA receptor reduces spontaneous activity of the GPe neurons (Kita et al., 2004) and stimulation of STN produces NMDA receptor-dependent slow excitatory postsynaptic potentials in GPe neurons (Kita and Kitai, 1991). However, no effect of NMDA antagonists on discharge rate or pattern of GPe neurons has been seen when STN inputs are severed (Chan et al., 2004). Thus, although the firing of GPe neurons appears to be autonomous, it may be modulated by glutamatergic inputs. Overall, previous studies suggest functional expression of NMDA receptors in GPe neurons. Nonetheless, the subtypes of NMDA receptors and the GPe cell-type specific pattern of expression is unknown. This is important because the different NMDA receptor subtypes can contribute uniquely to the neuronal excitability and may have different roles in pathological conditions. In particular, GluN2C and GluN2D receptors have unusual biophysical and pharmacological properties such that they are less sensitive to Mg^{2+}-block and have high glutamate/glycine

affinity and do not exhibit any desensitization (Traynelis et al., 2010). Therefore, GluN2C/GluN2D receptors may contribute significantly to neuronal excitability and to tonic bursting.

We have recently shown that the GluN2C subunit is expressed in unique cell populations in specific brain regions (Ravikrishnan et al., 2018). We have found expression of GluN2C subunit in the PV neurons in GPe but its functional significance remains unknown. Growing evidence points to altered physiology of GPe in movement disorders including Parkinson's (PD) and Huntington's disease (HD) (Gittis et al., 2014; Hegeman et al., 2016). Importantly, recent studies have demonstrated that optogenetic enhancement of PV neuron function in the GPe rescues motor deficits in a mouse model of PD (Mastro et al., 2017). In this study, we examined the role of GluN2C-containing receptors in the GPe in the regulation of neuronal activity and effect on motor function in a mouse model of PD. Our results demonstrate that pharmacological potentiation of GluN2C-containing receptors increases firing of GPe neurons and alleviates motor deficits in a hemiparkinsonian mouse model.

2. Materials and methods

2.1. Animals

For electrophysiology and biochemistry studies wildtype or Grin2C$^{tm1(EGFP/cre/ERT2)Wtsi}$ mouse line on pure C57BL/6 N background were used (Ravikrishnan et al., 2018; Shelkar et al., 2019; Liu et al., 2019). Conditional deletion of GluN2D from PV neurons was achieved by crossing PV-Cre mouse line (Jax stock number 017320) with GluN2D$^{flox/flox}$ mice. The GluN2D$^{flox/flox}$ mice were generated by removing the reporter cassette by crossing Grin2D$^{tm1a(EUCOMM)Wtsi}$ mice from Wellcome Trust Sanger Institute with B6-SJL-Tg(ACTFLPe) 9205Dym/J line. Mice were group-housed on a 12:12 light/dark cycle with ad libitum access to food and water. Procedures were approved by the Creighton University Institutional Animal Care and Use Committee and conformed to the NIH Guide for the Care and Use of Laboratory Animals. For behavioral studies male Swiss albino mice (25–30 g; 5–6 weeks) were used. Animals were procured from National Institute of Nutrition, Hyderabad, India. Experimental procedures were approved by the Institutional Animal Ethical Committee (IAEC/UDPS/2018/7) and executed strictly according to the guidelines of Committee for the Purpose of Control and Supervision of Experiments on Animals, Government of India.

2.2. Drugs

For electrophysiology studies DQP-1105 (Tocris, Minneapolis, MN, USA), D-cycloserine (DCS) (Sigma-Aldrich, St. Louis, MO, USA), AICP and + CIQ (Brandt Labs LLC, Atlanta GA, USA) stocks were made in either distilled water or DMSO and then diluted in recording buffer. AICP was prepared in the laboratory of Dr. Rasmus Clausen (University of Copenhagen). Tamoxifen (Sigma-Aldrich, St. Louis, MO, USA) was dissolved in corn oil (Sigma-Aldrich, St. Louis, MO, USA) at a concentration of 20 mg/ml by shaking overnight at 37 °C. For behavioral studies, 6-OHDA hydrochloride (Sigma-Aldrich, St. Louis, MO, USA) for intra-striatal injection was dissolved in 0.9% saline solution containing 0.2% ascorbic acid. Final concentration was 2 μg/μl. DCS (Sigma-Aldrich, St. Louis, MO, USA)

was dissolved in 0.9% saline solution. AICP stock was prepared in DMSO and then further diluted to the final working concentration with PEG400 (0.5–1% *v*/v DMSO in PEG400).

2.3. Electrophysiology

Whole-cell electrophysiology was performed as previously described from 25 to 35 day old mice (Gupta et al., 2015; Gupta et al., 2016). After isoflurane anesthesia, mice were decapitated and brains were removed rapidly and placed in ice-cold artificial cerebrospinal fluid (ACSF) of the following composition (in mM): 130 NaCl, 24 $NaHCO_3$, 3.5 KCl, 1.25 NaH_2PO_4, 2.4 $CaCl_2$, 2.5 $MgCl_2$ and 10 glucose saturated with 95% O_2/5% CO_2. 300 μm thick parasagittal sections were prepared using vibrating microtome (Leica VT1200, Buffalo Grove, IL, USA). Cell attached or whole-cell patch recordings were obtained from neurons in GPe in current-clamp or voltage-clamp configurations with an Axopatch 200B (Molecular Devices, Sunnyvale, CA, USA). Glass pipettes with a resistance of 3–5 mOhm were used. Signal was filtered at 2 kHz and digitized at10 kHz using an Axon Digidata 1440A analog-to-digital board (Molecular Devices, CA). Whole-cell recordings with a pipette access resistance less than 20 mOhm and that changed less than 20% during the duration of recording were included. For cell-attached and whole-cell current-clamp recordings, patch pipettes were filled with a solution containing (in mM) 105 K-gluconate, 30 KCl, 10 HEPES, 10 Na_2-phosphocreatine, 4 Na_2ATP, and 0.3 Na_2GTP (pH 7.2). Spontaneous firings were recorded and analyzed with Minianalysis software (Synaposoft, Atlanta, GA, USA). For voltage-clamp recordings, glass pipettes were filled with an internal solution consisting of (in mM) 126 cesium methanesulfonate, 8 NaCl, 10 HEPES, 8 Na_2-phosphocreatine, 0.3 Na_2GTP, 4 MgATP, 0.1 $CaCl_2$, 1 EGTA (pH 7.3). Additionally, 2.9 mM QX-314 was added to block voltage-gated sodium channels in recorded cells. Electrical-evoked NMDA currents were induced by a bipolar tungsten electrode (TST33A001KT, World Precision Instruments) placed posterior to the recorded neurons in the presence of 100 μM picrotoxin and 10 μM CNQX. The extracellular $MgCl_2$ was reduced to 0.2 mM. For puffing-induced NMDA currents, a picospritzer was used to evoke currents by pressure applying brief pulses (100 to 300 ms, 9 to 12 psi) of 1 mM NMDA through a borosilicate capillary tube in the presence of 100 μM picrotoxin and 10 μM CNQX in extracellular solution.

2.4. Immunohistochemistry

Immunohistochemistry was performed as previously described (Ravikrishnan et al., 2018; Liu et al., 2019). Briefly, mice were transcardially perfused, brains were collected and cryoprotected and stored at − 80 °C. The brains were cut in coronal plane and sections passing through striatum, GPe or nucleus reticularis of the thalamus (nRT) were collected. After washing with PBT (0.25% Triton-X in 0.01 M PB), sections were incubated in appropriate blocking solution containing 10% normal goat serum or normal donkey serum in PBT for 1 h at room temperature. Following blocking, sections were incubated in primary antibodies at appropriate concentrations (chicken anti-GFP, 1:1000, Invitrogen A10262; rabbit anti-parvalbumin, 1:5000, Swant PV27; chicken anti-TH, 1:500, Aves lab TYH) in solution containing 5% normal goat serum or donkey serum in PBT for overnight at 4 °C. On the next day, sections were washed and thereafter incubated with the appropriate secondary antibodies conjugated to DyLight 488 (goat anti-chicken IgG-conjugated, KPL, 1:500 in PBT), AlexaFluor 594 (goat anti-rabbit 1:500 in PBT), or AlexaFluor 488 (donkey

anti-rabbit 1:500 in PBT) for 2 h at room temperature. Sections were then washed and mounted with Fluoromount-G (SouthernBiotech, AL, USA). Images were acquired with an Infinity camera (Lumenera Co., Ontario, Canada) coupled to a widefield epifluorescence microscope (Nikon Eclipse Ci) using the Lumenera Infinity Analyze software (Lumenera Co.). For confocal images equivalent regions, 1024 × 1024 pixels, were captured using a Nikon Ti-E inverted microscope with a Yokagawa spinning disc for confocal imaging. The colocalization of EGFP (GluN2C) with PV or mCherry with PV was counted manually using NIH Image J software. Immunohistochemistry results were confirmed in at least three mice. For lesion, tracing and cannula verification studies, images were captured using Olympus VS120 Virtual Slide Scanning microscope.

2.5. Adeno-associated virus injections and tamoxifen treatment

To identify cell specific expression of GluN2C-containing NMDA receptors in GPe and nRT, and for mapping output pathways, we used Grin2C$^{tm1(EGFP/cre/ERT2)Wtsi}$ reporter mice (Wellcome Trust Sanger Institute; (Ravikrishnan et al., 2018)) which allows expression of tamoxifen-inducible Cre. For the virus injections, mice were anaesthetized, and a small hole was drilled above the GPe (− 0.4 mm posterior, − 1.75 mm lateral, and − 3.75 mm ventral with respect to bregma). The virus particles AAV5/EF1αa-DIO-mCherry (UNC vector core, Chapel Hill, NC, USA) were injected (100nl) using a microliter syringe (NanoFil; World Precision Instruments, Sarasota, FL) with 33-gauge needle (NF33BV-2; World Precision Instruments) at a rate of 1 nl/s using a UMP3 micro-syringe pump (World Precision Instruments). The coordinates used for injection into nRT were − 0.2 mm posterior, 1.6 mm lateral, and − 3.5 mm ventral. After 2 weeks of surgery, these mice were injected with tamoxifen (75 mg/kg, ip) once-in-a day for 5 days. The animals were sacrificed 1 month after the last dose of tamoxifen and brains were processed for immunohistochemistry.

2.6. Tissue preparation and western blotting

Total protein samples were prepared from GPe tissue and western blotting was conducted as previously described (Shelkar et al., 2019). Briefly, samples were resolved on SDS-PAGE gel and transferred onto nitrocellulose membrane. Membranes were blocked with 5% dry milk in Tris-buffered saline/Tween 20 (TBST) at room temperature for 1h and incubated with appropriate primary antibodies GluN2C: Neuromab, 75–411; RRID: AB_2531892 at 1:1000; GluN1: Frontiers Institute, AF720 at 1:1000; GluN2A: Millipore, AB1555P at 1:1000; GluN2B: Millipore, 06–600 at 1:1000; GluN2D: Millipore, MAB5578 at 1:1000; GAPDH: Millipore, MAB374 at 1:2000 and β-actin: Santa Cruz Biotechnology, sc-69,879, 1:4000) for overnight at 4°C. The blots were incubated in horse-radish peroxidase conjugated anti-mouse (Jackson ImmunoResearch, #115–035–003, 1:10000) or anti-rabbit secondary antibody (Jackson ImmunoResearch, #111–035–003, 1:10000) in 5% dry milk solution in TBST for 1h at room temperature followed by washing with TBST. Blots were developed using SuperSignal® West Pico chemiluminescent substrate (Thermo Scientific, Rockford, IL, USA) and processed using X-ray film processor model-BMI No 122106 (Brown's Medical imaging, Omaha, NE, USA) or ChemiDoc imaging system (Bio-Rad Laboratories, Inc., USA). The representative blots shown were not modified for exposure or contrast from the original X-ray films and were not assembled from cropped images.

2.7. Hemiparkinsonian model

To achieve unilateral lesion of the nigrostriatal system, mice received 6-OHDA hydrochloride injections into the left striatum. Mice were anaesthetized using thiopental sodium (Neon Laboratories Ltd), 45 mg/kg, ip and placed into a stereotactic frame with nose and ear bars specially adapted for mice (David Kopf Instruments, USA). 6-OHDA was dissolved at a concentration of 2 μg/μl saline in 0.2% ascorbic acid and injected at a volume of 3 μl resulting in final dosage of 6 μg. The lesion was performed using a Hamilton syringe at the following coordinates: +0.65 mm anterior; 2.00 mm lateral to midline; 3.00 mm ventral with respect to the bregma. The injection was conducted at a rate 0.5 μl/min and the needle was left in place for another 5 min after the injection before it was slowly drawn back. Whereas, sham group received 0.2% ascorbic acid in saline at the same rate. Behavioral impairment was used as a criterion for inclusion of 6-OHDA injected animals. After completion of behavioral tests mice were sacrificed and brains collected for immunohistochemical analysis of tyrosine hydroxylase in the striatum. A reduction of 64.3% in the intensity of tyrosine hydroxylase staining was observed in lesioned animals (mean fluorescent intensity in striatum of sham = 12.73 ± 0.78, $n = 6$ and lesioned = 4.54 ± 0.23, $n = 30$). The group sizes for behavioral experiments were based on power analysis using preliminary data.

2.8. Cannula implantation surgery

After injecting 6-OHDA, guide cannula was stereotaxically implanted ipsilaterally into the GPe as per the coordinates, 0.7 mm posterior, 1.9 mm lateral and 3.1 mm ventral with respect to bregma and was secured to the skull using mounting screws and dental cement (DPI-RR Cold Cure, acrylic powder, Dental Product of India, Mumbai, India). A dummy cannula was used to occlude the guide cannula, when not in use. The animals were then allowed to recover for a week using daily treated with 0.2 ml of the antibiotic sodium cefotaxime (262 mg/ml, ip).

2.9. Behavioral assessment

Two weeks after induction of 6-OHDA lesion in mice, NMDA receptor drug treatments were done using a Hamilton syringe attached to injection cannula through PE10 tubing. DCS (10, 30 and 50 μg in a volume of 1 μl) or AICP (100 ng in a volume of 0.3 μl) was administered at a rate of 1 μl/min into the GPe. The injection cannula was left in place for further 2 min before being slowly withdrawn to avoid backflow. All paradigms were performed after 15 min of drug administration in different group of animals. At the end of an experiment, animals were euthanized by pentobarbitone (60 mg/kg, ip) overdose and brain were collected and processed to assess cannula placement.

2.10. Locomotor activity and ipsilateral rotations

Locomotor activity was recorded in a 25.4 × 25.4 cm open field (OFT) area made of acrylic white wall and divided into 24 sections (V.J. Instruments, India). For the open field test (OFT), mouse was placed in the center of the arena and number of squares crossed by the four paws (locomotor activity) was recorded manually for 5 min (Gawai et al., 2020). The

arena was cleaned with 70% alcohol between trials. Ipsilateral rotations were recorded with locomotor activity in the same animals.

2.11. Wire hanging test

Wire hanging test was performed to assess the neuromuscular ability of mice. Animals were suspended by its fore paws with a 2 mm wire 30 cm above the ground. Latency to fall was measured. Five trials for each mouse with a 60 s inter-trial interval were conducted, and a mean value was calculated.

2.12. Beam walk test

Motor performance was measured with beam walk test. Mice were trained for three days to traverse the beam before 6-OHDA lesion. Apparatus consisted of a square beam (2.5 cm wide, 122 cm long, at a height of 42 cm) connected to a black box (20.5 cm × 25 cm × 25 cm). A bright light was placed above the start point to motivate the mice to traverse the beam. Performance was rated as follows: The mice not able to stay on the beam = 0, the mice did not move, but was able to stay on the beam = 1, the mice traversed the beam with more than 50% foot slips of the affected hind limb = 2, the mice traversed the beam with more than one foot slip, but less than 50% = 3, the mice had only one slip of the hind limb = 4, and the mice traversed the beam without any slips of the hind limb = 5.

2.13. Statistical analysis

The results were analyzed by paired or unpaired *t*-test or one-way or two-way ANOVA followed by post-hoc Tukey's or Bonferroni's multiple comparison test. The significance level of $p < 0.05$ was considered statistically significant. All data were presented as mean ± SEM.

3. Results

3.1. Fast spiking neurons in the GPe are regulated by NMDA receptors

We first evaluated the firing pattern of neurons in GPe. It has recently been demonstrated that GPe is composed of at least three different types of inhibitory neurons including PV, arkypallidal and Npas1+ (Hernandez et al., 2015; Mallet et al., 2012), which can be differentiated based on their firing properties. In cell-attached recordings we found that majority of cells could be grouped into three categories namely fast regular, slow regular and slow irregular (Fig. 1A). The regular fast spiking neurons have been previously demonstrated to represent the PV neurons. We primarily used this characteristic for identifying cell type. There are also differences in hyperpolarization sag and hyperpolarization-induced rebound action potential noted previously in different cell-types (Hernandez et al., 2015). We observed lower sag in fast spiking neurons, however this characteristic was not consistent across the cells. We next confirmed that firing in regular fast-spiking neuron is dependent on NMDA receptor function. NMDA receptor competitive antagonist AP5 (100 μM) reduced the firing of regular fast spiking neurons (Fig. 1B; baseline 100.8 ± 3.10% vs. 100 μM AP5 73.3 ± 7.34%, $p = 0.028$, Paired *t*-test). To address potential contribution of GluN2C/2D-containing receptors to the NMDA receptor current in the GPe we next examined the sensitivity of firing of regular fast spiking neurons to

GluN2C/2D receptor antagonist DQP-1105 (Acker et al., 2011). The firing of GPe fast spiking neurons in cell-attached mode was reduced by DQP-1105 (Fig. 1B; baseline 99.7 ± 2.66% vs. 20 μM DQP1105 79.4 ± 7.87%, $p = 0.029$, Paired t-test), to approximately similar level as that by AP5 suggesting a contribution of GluN2C/2D-containing NMDA receptors to basal firing. We also examined the contribution of GluN2C/2D-containing receptors to NMDA receptor current in GPe fast spiking neurons. GPe fast spiking neurons showed evoked NMDA receptor currents upon stimulation of fiber inputs from STN (Fig. 1C). Furthermore, we found that application of DQP-1105 reduced NMDA receptor currents obtained at − 40 mV by approximately 25% suggesting contribution by GluN2C/2D-containing receptors under basal conditions (Fig. 1D).

3.2. Novel reporter model demonstrates expression of GluN2C subunit in PV neurons in GPe

We have previously used a reporter model to address the localization of GluN2C subunit in CNS (Ravikrishnan et al., 2018). Using this reporter model, we first established that GluN2C subunit is expressed in the GPe. Similar to our previous results we found EGFP (GluN2C) expression in the GPe primarily localized to PV neurons (Fig. 2A). We also evaluated expression of GluN2C by western blotting using total protein preparation from GPe tissue of wildtype and GluN2C KO mice. Strong expression of GluN2C was observed in the GPe in wildtype mice (Fig. 2B). In addition, expression of the obligatory GluN1 subunit was also observed in the GPe protein lysate. No change in GluN1 expression was noted in the GluN2C KO. The Grin2C mouse model also has a CreERT2 cassette along with the reporter. We tested whether cre expression was also localized primarily to PV cell types. As described in the methods for these experiments Grin2C-EGFP-CreERT2 mice were injected with cre-dependent-mCherry AAV into the GPe region. After sufficient time for AAV expression, Cre recombinase was induced by ip injection of tamoxifen and after an interval of several weeks brain tissue was collected and analyzed for expression of cre-dependent mCherry in the GPe and labeled terminal projections in the STN. We observed a large population of mCherry-positive neurons in GPe that colocalized with PV neurons (Fig. 2C). Neurons with mCherry-alone and PV-alone labeling were also observed in the GPe suggesting that although majority of GluN2C subunit is localized to PV neurons, GluN2C may also express in a subset of non-PV cells. We also observed labeled terminals in the STN (Fig. 2D) consistent with previous reports that PV neurons in the GPe project to STN (Gittis et al., 2014; Hegeman et al., 2016). We further examined nRT, where GluN2C is known to be enriched, using a similar cre-dependent approach to further establish the Grin2c model. AAV containing Cre-dependent mCherry reporter was injected into the nRT and after sufficient time for expression followed by tamoxifen administration tissue was collected and examined by histochemistry. Neurons labeled with cre-dependent reporter mCherry were observed in the nRT that colocalized with PV neurons (Supplementary Fig. 1A–C). The nRT projects to several thalamic nuclei particularly ventrobasal thalamus. Consistent with this, labeled projections were observed in ventrobasal thalamus and other thalamic nuclei (Supplementary Fig. 1D). Together, these results demonstrate that the CreERT2 cassette provides robust labeling in this mouse model and may be used for cre-dependent studies. We next evaluated whether GluN2C deletion affected the firing rate of regular fast spiking neurons. No significant difference in the firing rate was observed in fast spiking neurons in

GluN2C KO compared to wildtype (Fig. 2E). In addition, no significant change was observed in firing rate of all GPe neurons when all cell types were pooled (Fig. 2E). Thus, loss of GluN2C subunit does not appear to affect the basal firing of GPe neurons. We also examined whether loss of GluN2C subunit affects expression of other NMDA receptor subunits in the GPe. Total lysates from GPe was examined. Expression of the obligatory subunit GluN1 was observed in GPe. Importantly, expression of GluN2A, GluN2B and GluN2D was also obesrved. No significant change in the expression of these subunits was observed in the GluN2C KO (Fig. 3A). We next examined whether PV neurons also express GluN2D subunit which share some biophysical and pharmacological properties with GluN2C-containing receptors. In order to address this we used a conditional strategy to selectively deleted GluN2D from PV neurons (Fig. 3B). In this model we found a signficant reduction in GluN2D expression demonstrating that GluN2D is also expressed in PV neurons. Thus, it is possible that some of the pharmacological effects especially with drugs that are non-selective for GluN2C and GluN2D receptors may arise due to GluN2D-containing receptors.

3.3. D-cycloserine potentiates the firing of fast spiking neurons in the GPe in a GluN2C-dependent manner

In order to test whether GluN2C subunit may contribute to NMDA receptor currents and firing of fast spiking neurons in the GPe we used a pharmacological approach. DCS is a co-agonist of the NMDA receptor that binds to the glycine-site. DCS exhibit GluN2-subtype dependent efficacy and approximately 2-fold higher efficacy than endogenous glycine or D-serine at GluN1/GluN2C receptors (Dravid et al., 2010; Sheinin et al., 2001). In cell-attached mode we examined the firing pattern of individual neurons and thereafter whole-cell recordings were conducted from the same neurons. DCS application increased the whole-cell currents from fast spiking neurons (Fig. 4A; baseline 99.58 ± 1.42% vs. 100 μM DCS 178.7 ± 28.95%, $N = 6$, $*p = 0.0443$, Paired *t*-test). We also found a slight increase in the currents in non-fast spiking neurons however, this was smaller than from fast-spiking neurons (Fig. 4B; baseline 100.8 ± 2.0% vs. 100 μM DCS 118.2 ± 7.3%, $p = 0.0648$, Paired t-test). We further evaluated the effect of DCS on GPe neuron firing. Application of 100 μM DCS led to a significant increase in firing rate in fast spiking neurons and this was dependent on GluN2C subunit since no increase was observed in GluN2C knockout (Fig. 4C; WT: baseline 98.16 ± 2.43% vs. 100 μM DCS 194.32 ± 34.49%, $p = 0.007$; GluN2C KO: baseline 102.96 ± 3.37% vs. 100 μM DCS 98.05 ± 4.22%, $p > 0.999$; Two-way ANOVA with Bonferroni's post-hoc test). These results suggest that GluN2C subunit may contribute to currents in both fast spiking and non-fast spiking neurons, but it may have a greater contribution to NMDA currents in fast spiking neurons. Furthermore, facilitation of GluN2C-containing receptors increases the firing of fast spiking neurons.

3.4. Novel superagonist of GluN2C-containing receptors AICP increases the firing of fast spiking neurons in a GluN2C-dependent manner

We next examined the effect of a novel superagonist of GluN2C-containing receptors AICP on the firing of fast spiking neurons. AICP, similar to DCS, is a co-agonist GluN1 binding ligand that increases the function of GluN2C-containing receptors by ~3.5-fold (Jessen et al., 2017). We found that 1 μM AICP increased the firing of fast spiking neurons in GPe and

this effect was absent in GluN2C knockout model (Fig. 5A; WT: baseline 100.02 ± 1.41% vs. 1 μM AICP 147.91 ± 18.71%, $p = 0.0065$; GluN2C KO: baseline 101.45 ± 1.32% vs. 1 μM AICP 117.83 ± 13.39%, $p = 0.657$; Two-way ANOVA with Bonferroni's post-hoc test). We also evaluated the effect of a positive allosteric modulator for GluN2C/2D-containing receptors (+)CIQ (Mullasseril et al., 2010; Santangelo Freel et al., 2013) on GPe neuron firing. Bath application of 20 μM (+)CIQ increased the firing of fast spiking neurons (Fig. 4B; Baseline; 100.7 ± 1.8 vs (+) CIQ; 137.3 ± 11.51, $p = 0.0244$, paired *t*-test).

3.5. D-cycloserine and AICP administration into the GPe improves motor function in a hemiparkinsonian model

We finally tested whether facilitation of activity of GluN2C-containing receptors in the GPe improves motor function in a hemiparkinsonian model. Unilateral lesion for the dorsal striatum was induced by 6-OHDA. The loss of dopaminergic terminals was confirmed in this model using TH staining (Fig. 6A) and the presence of ipsilateral rotations. After a recovery period form 6-OHDA lesion and cannula implantation surgery, the effect of DCS (10, 30 and 50 μg) and AICP (100 ng) infusion into the GPe on the same side of the lesion was evaluated on motor function. Lesion by 6-OHDA led to a significant decline in total locomotor activity (Fig. 6B; Sham 111 ± 7.285 crossing per 5 min vs 6-OHDA 37.33 ± 4.44 crossing per 5 min, $p < 0.0001$; One-way ANOVA with Bonferroni's post-hoc test) and an increase in ipsilateral rotations in the open field test (Fig. 6C; Sham 1 ± 0.5164 vs 6-OHDA 3.333 ± 0.667, $p = 0.0316$; One-way ANOVA with Bonferroni's post-hoc test). DCS (30 and 50 μg) and AICP increased the locomotor activity in 6-OHDA model (6-OHDA 37.33 ± 4.44 crossing per 5 min vs DCS 30 μg 73.17 ± 7.964 crossing per 5 min, $p = 0.01$; 6-OHDA vs DCS 50 μg 75.67 ± 8.991 crossing per 5 min, $p = 0.0099$; 6-OHDA vs AICP 90.33 ± 8.11 crossing per 5 min, $p = 0.0002$; One-way ANOVA with Bonferroni's post-hoc test). Ipsilateral rotations were also reduced by DCS and AICP, but this effect did not reach significance. Further evaluation of motor function in 6-OHDA lesioned animals demonstrated reduced latency to fall in the hanging wire test which was significantly improved by AICP (Fig. 6D; Sham 139.3 ± 15.37 s vs 6-OHDA 43.833 ± 6.145 s, $p < 0.0001$; 6-OHDA vs AICP 106.2 ± 4.483 s, $p = 0.0014$; One-way ANOVA with Bonferroni's post-hoc test). The beam walk score reduced by 6-OHDA lesion was significantly improved by DCS (50 μg) and AICP (Fig. 6E; Sham 4.667 ± 0.2108 vs 6-OHDA 1.833 ± 0.307, $p < 0.0001$; 6-OHDA vs DCS 50 μg 3.333 ± 0.333, $p = 0.031$; 6-OHDA vs AICP 3.833 ± 0.307, $p = 0.001$; One-way ANOVA with Bonferroni's post-hoc test). These behavioral improvements by DCS and AICP were specific to the 6-OHDA animals since DCS or AICP administration in GPe of unlesioned mice did not affect these behaviors (Fig. 6F–I). In addition, we have previously shown that intracerebroventricular injection of AICP does not affect basal locomotor activity in normal mice (Liu et al., 2019). Together, electrophysiology and behavioral results demonstrate that DCS and AICP improves motor function in a mouse model of PD by facilitating the function of GluN2C-containing NMDA receptors in the GPe.

4. Discussion

4.1. Distribution of GluN2C subunit in the globus pallidus externa

GPe was originally considered as a homogenous group of GABAergic neurons projecting to the STN as part of the indirect basal ganglia pathway. Recent studies have however identified neurochemically distinct subtypes of neurons in the GPe that project to different nuclei of the basal ganglia circuitry and may play a distinct role in motor functions (Gittis et al., 2014; Hegeman et al., 2016). Importantly, a subgroup of GPe neurons defined by their expression of PV was found to play an important role in PD pathology, since optogenetic enhancement of these cells improved motor function in a mouse model of PD (Mastro et al., 2017). In this study, with multiple lines of evidences, we demonstrate the expression of functional GluN2C-containing receptors in the GPe.

First, the GPe neurons were sensitive to GluN2C/2D inhibitor DQP-1105 and glycine-site agonists DCS and AICP that have higher efficacy for GluN2C-containing receptors. The increase in NMDA receptor currents by DCS was more robust in fast-spiking GPe neurons. Secondly, using a EGFP-CreERT2 reporter model, we found expression of EGFP or cre-dependent mCherry reporter in the GPe, particularly in PV neurons. Western blotting analysis also demonstrated strong expression of GluN2C subunit in the GPe. Third, we found an increase in firing of fast spiking neuron by DCS and AICP in brain slices from wildtype but not GluN2C KO mice. Overall, we found robust expression of GluN2C-containing receptors in the GPe PV neurons and facilitation of their function was found to increase spontaneous firing of fast spiking neurons. This is the first subtype specific assessment of NMDA receptors in the GPe relevant to spontaneous firing observed in the neurons in this region.

Several other key conclusions can be drawn from these results. First, GluN2C subunit may not contribute significantly to the basal firing of GPe neurons because ablation of GluN2C subunit did not affect the normal firing frequency. Alternatively, compensatory mechanisms may result in a lack of effect of ablation of GluN2C subunit. In contrast, facilitation of GluN2C-containing receptors increases the firing of GPe fast spiking neurons. We have recently shown that in the nRT neurons, GluN2C ablation similarly does not affect basal excitability and burst firing, but facilitation of GluN2C-containing receptors by AICP modulates these properties (Liu et al., 2019). Thus, it appears that increasing ongoing activity of GluN2C-containing receptors can modulate neuronal function. It should be noted that unlike the nRT neurons, GPe neurons responded to both DCS and CIQ suggesting potentially different levels of basal GluN2C activity or requirement for neuronal modulation. Another important conclusion from our studies is regarding the Grin2C-creERT2 model. Previous study has shown the utility of the Grin2C-creERT2 mouse line for inducible cre expression for in vitro studies in suprachiasmatic nucleus neurons (Brancaccio et al., 2017). Here we demonstrate that tamoxifen-inducible cre expression occurs in vivo and in several forebrain regions including GPe and nRT in a robust manner. Given the unique cell type specific expression of GluN2C in various brain regions (Ravikrishnan et al., 2018; Alsaad et al., 2019), the inducible cre model may be useful for other applications.

We also assessed the expression of other GluN2 subunits in the GPe and found that all subunits are expressed in the GPe. The expression of GluN2D is particularly interesting due to some similarity in the biophysical properties with GluN2C-containing receptors. In addition, the pharmacological tools used particularly DQP1105 inhibits GluN2D-containing receptors with higher affinity. Using conditional deletion model we found that GluN2D subunit may also expressed in the PV neurons in the GPe. Thus, it is likely that some of the effect of the pharmacological tools used in this study may arise due to effect on GluN2D-containing receptors. Nonetheless, because DCS and AICP did not produce significant increase in firing in GluN2C KO and since there were no changes in the other GluN2 subunit expression in GluN2C KO, it can be concluded that GluN2C-containing receptors play an important functional role in GPe neuron physiology. Further experiments are necessary to understand the contribution of GluN2D-containing receptors in GPe function. This is particularly interesting because GluN2D subunit is also expressed in the STN and the reciprocal interaction between GPe and STN regulates oscillatory activity relevant to GluN2D subunits.

4.2. Mechanism of motor improvement by facilitating GluN2C-containing receptors in the globus pallidus externa

We also found that administration of DCS or AICP into the GPe improved motor function in a mouse model of PD. The doses of DCS and AICP that produced behavioral improvement were in line with their relative in vitro potency for activation of GluN2C-containing NMDA receptors (Jessen et al., 2017). The effect of DCS or AICP may simply be due to the increase in PV neuron mediated GPe-STN connectivity. Indeed, hypoactivity of the GPe has been proposed to contribute to the hyperactivity of the output nuclei, giving rise to akinesia in PD (Albin et al., 1989; DeLong, 1990; Crossman, 1989). It has also been shown that high frequency stimulation of GPe neurons in MPTP monkeys can contribute to the relief of bradykinesia (Vitek and Johnson, 2019). In fact, studies have shown that GPe neurons project mainly to the STN (Kita, 2007; Kita and Kita, 2001; Mallet et al., 2012), and the hyperactivity of the STN in parkinsonism may be caused at least in part by the specific loss of pallidal neurons projecting to this nucleus. Moreover, recently optogenetic stimulation of PV-expressing GPe neurons has been shown to restore movement in dopamine-depleted mice (Mastro et al., 2017). Alternatively, it is possible that DCS or AICP may produce changes in dopamine level. Severe loss of dopamine and its metabolites as well as dopaminergic fibres within the GPe have been observed in human patients and animal models of PD (Jan et al., 2000; Rajput et al., 2008). Further, local activation of dopamine receptors in the GPe increased locomotor activity, while its blockade produced profound akinesia (Costall et al., 1972; Hauber and Lutz, 1999). We found that, in addition to locomotion, other dopamine mediated behaviors including ipsilateral rotations, wire hanging and beam walk were also improved by DCS and AICP. Thus, it is conceivable that facilitating the function of GluN2C-containing NMDA receptor may indirectly increase the dopamine levels in GPe to improve the parkinsonian-like symptoms in 6-OHDA treated animals. Assessment of dopamine levels after treatment with DCS or AICP can provide more details regarding the specific mechanism.

Another function attributed to GPe and relevant to motor disorders is its role in generating oscillations. The interconnections between basal ganglia nuclei such as STN and striatum with GPe has been found to be responsible for oscillatory activity. Importantly, an increase in β frequency oscillations is observed in PD and PD models and GPe-STN loop is thought to be critical for generation of these oscillations (Guridi and Alegre, 2017; Mallet et al., 2008; Holgado et al., 2010; Ahn et al., 2016; Kovaleski et al., 2020). We have identified that GluN2C subunits may modulate cortical oscillations (Gupta et al., 2016). Specifically GluN2C knockout mice exhibit an increase in cortical oscillation in the β frequency and NMDA receptor channel blocker induced gamma oscillations are exaggerated in GluN2C knockout mice (Gupta et al., 2016; Mao et al., 2020). Although the precise mechanism underlying modulation of oscillations in GluN2C knockout are not known, it is possible that GPe may contribute to these changes. Indeed, the basally active nature of GluN2C-containing receptors due to lower Mg^{2+}-sensitivity and lack of desensitization are ideal for tonic oscillatory regulation. Similarly, our studies also demonstrate potential expression of GluN2D subunit in the PV neurons in the GPe. This together with the known expression of GluN2D in STN (Swanger et al., 2015), implicate that GluN2D-containing receptors may play a major role in oscillatory activity in the basal ganglia circuitry. We propose that beyond the results presented in this study, GluN2C-containing receptors may regulate not only the motor function but also overall basal ganglia connectivity and oscillations and represent important targets for motor disorders. With the ongoing discovery of GluN2C-selective agents and a better understanding of the GluN2C-containing receptor expression and function it is likely that this mechanism may have therapeutic utility for PD and other motor disorders.

Supplementary Material

Refer to Web version on PubMed Central for supplementary material.

Acknowledgements

The authors are thankful to Lorenzo Rivera and Ratnamala Uppala for excellent technical help.

Funding/disclosures

This work was supported by grants from the NSF1456818 (SMD), NIH NS104705 (SMD), NIH NS118731 and NIH MH116003 (SMD).

References

Abdi A, Mallet N, Mohamed FY, Sharott A, Dodson PD, Nakamura KC, Suri S, Avery SV, Larvin JT, Garas FN, Garas SN, Vinciati F, Morin S, Bezard E, Baufreton J, Magill PJ, 2015. Prototypic and arkypallidal neurons in the dopamine-intact external globus pallidus. J. Neurosci 35, 6667–6688. [PubMed: 25926446]

Acker TM, Yuan H, Hansen KB, Vance KM, Ogden KK, Jensen HS, Burger PB, Mullasseril P, Snyder JP, Liotta DC, Traynelis SF, 2011. Mechanism for noncompetitive inhibition by novel GluN2C/D N-methyl-D-aspartate receptor subunit-selective modulators. Mol. Pharmacol 80, 782–795. [PubMed: 21807990]

Ahn S, Zauber SE, Worth RM, Rubchinsky LL, 2016. Synchronized Beta-band oscillations in a model of the Globus pallidus-subthalamic nucleus network under external input. Front. Comput. Neurosci 10, 134. [PubMed: 28066222]

Albin RL, Young AB, Penney JB, 1989. The functional anatomy of basal ganglia disorders. Trends Neurosci. 12, 366–375. [PubMed: 2479133]

Alsaad HA, DeKorver NW, Mao Z, Dravid SM, Arikkath J, Monaghan DT, 2019. In the telencephalon, GluN2C NMDA receptor subunit mRNA is predominately expressed in glial cells and GluN2D mRNA in interneurons. Neurochem. Res 44, 61–77. [PubMed: 29651654]

Brancaccio M, Patton AP, Chesham JE, Maywood ES, Hastings MH, 2017. Astrocytes control circadian timekeeping in the suprachiasmatic nucleus via glutamatergic signaling. Neuron 93, 1420–1435.e5. [PubMed: 28285822]

Chan CS, Shigemoto R, Mercer JN, Surmeier DJ, 2004. HCN2 and HCN1 channels govern the regularity of autonomous pacemaking and synaptic resetting in globus pallidus neurons. J. Neurosci 24, 9921–9932. [PubMed: 15525777]

Costall B, Naylor RJ, Olley JE, 1972. On the involvement of the caudate-putamen, globus pallidus and substantia nigra with neuroleptic and cholinergic modification of locomotor activity. Neuropharmacology 11, 317–330. [PubMed: 5050440]

Crossman AR, 1989. Neural mechanisms in disorders of movement. Comp. Biochem. Physiol. A. Comp. Physiol 93, 141–149. [PubMed: 2568216]

DeLong MR, 1971. Activity of pallidal neurons during movement. J. Neurophysiol 34, 414–427. [PubMed: 4997823]

DeLong MR, 1990. Primate models of movement disorders of basal ganglia origin. Trends Neurosci. 13, 281–285. [PubMed: 1695404]

Dravid SM, Burger PB, Prakash A, Geballe MT, Yadav R, Le P, Vellano K, Snyder JP, Traynelis SF, 2010. Structural determinants of D-cycloserine efficacy at the NR1/NR2C NMDA receptors. J. Neurosci 30, 2741–2754. [PubMed: 20164358]

Gawai P, Upadhyay R, Gakare SG, Sarode L, Dravid SM, Ugale RR, 2020. Antipsychotic-like profile of CIQ isomers in animal models of schizophrenia. Behav. Pharmacol 31, 524–534. [PubMed: 31860561]

Gittis AH, Berke JD, Bevan MD, Chan CS, Mallet N, Morrow MM, Schmidt R, 2014. New roles for the external globus pallidus in basal ganglia circuits and behavior. J. Neurosci 34, 15178–15183. [PubMed: 25392486]

Gupta SC, Yadav R, Pavuluri R, Morley BJ, Stairs DJ, Dravid SM, 2015. Essential role of GluD1 in dendritic spine development and GluN2B to GluN2A NMDAR subunit switch in the cortex and hippocampus reveals ability of GluN2B inhibition in correcting hyperconnectivity. Neuropharmacology 93, 274–284. [PubMed: 25721396]

Gupta SC, Ravikrishnan A, Liu J, Mao Z, Pavuluri R, Hillman BG, Gandhi PJ, Stairs DJ, Li M, Ugale RR, Monaghan DT, Dravid SM, 2016. The NMDA receptor GluN2C subunit controls cortical excitatory-inhibitory balance, neuronal oscillations and cognitive function. Sci. Rep 6, 38321. [PubMed: 27922130]

Guridi J, Alegre M, 2017. Oscillatory activity in the basal ganglia and deep brain stimulation. Mov. Disord 32, 64–69. [PubMed: 27548437]

Hauber W, Lutz S, 1999. Dopamine D1 or D2 receptor blockade in the globus pallidus produces akinesia in the rat. Behav. Brain Res 106, 143–150. [PubMed: 10595430]

Hegeman DJ, Hong ES, Hernandez VM, Chan CS, 2016. The external globus pallidus: progress and perspectives. Eur. J. Neurosci 43, 1239–1265. [PubMed: 26841063]

Hernandez VM, Hegeman DJ, Cui Q, Kelver DA, Fiske MP, Glajch KE, Pitt JE, Huang TY, Justice NJ, Chan CS, 2015. Parvalbumin+ neurons and Npas1+ neurons are distinct neuron classes in the mouse external globus pallidus. J. Neurosci 35, 11830–11847. [PubMed: 26311767]

Holgado AJ, Terry JR, Bogacz R, 2010. Conditions for the generation of beta oscillations in the subthalamic nucleus-globus pallidus network. J. Neurosci 30, 12340–12352. [PubMed: 20844130]

Jan C, Francois C, Tande D, Yelnik J, Tremblay L, Agid Y, Hirsch E, 2000. Dopaminergic innervation of the pallidum in the normal state, in MPTP-treated monkeys and in parkinsonian patients. Eur. J. Neurosci 12, 4525–4535. [PubMed: 11122363]

Jessen M, Frederiksen K, Yi F, Clausen RP, Hansen KB, Brauner-Osborne H, Kilburn P, Damholt A, 2017. Identification of AICP as a GluN2C-selective N-methyl-d-aspartate receptor superagonist at the GluN1 Glycine site. Mol. Pharmacol 92, 151–161. [PubMed: 28588066]

Kita H, 2007. Globus pallidus external segment. Prog. Brain Res 160, 111–133. [PubMed: 17499111]

Kita H, Kita T, 2001. Number, origins, and chemical types of rat pallidostriatal projection neurons. J. Comp. Neurol 437, 438–448. [PubMed: 11503145]

Kita H, Kitai ST, 1991. Intracellular study of rat globus pallidus neurons: membrane properties and responses to neostriatal, subthalamic and nigral stimulation. Brain Res. 564, 296–305. [PubMed: 1810628]

Kita H, Nambu A, Kaneda K, Tachibana Y, Takada M, 2004. Role of ionotropic glutamatergic and GABAergic inputs on the firing activity of neurons in the external pallidum in awake monkeys. J. Neurophysiol 92, 3069–3084. [PubMed: 15486427]

Kovaleski RF, Callahan JW, Chazalon M, Wokosin DL, Baufreton J, Bevan MD, 2020. Dysregulation of external globus pallidus-subthalamic nucleus network dynamics in parkinsonian mice during cortical slow-wave activity and activation. J. Physiol 598, 1897–1927. [PubMed: 32112413]

Liu J, Shelkar GP, Zhao F, Clausen RP, Dravid SM, 2019. Modulation of burst firing of neurons in nucleus reticularis of the thalamus by GluN2C-containing NMDA receptors. Mol. Pharmacol 96 (2), 193–203.

Mallet N, Pogosyan A, Marton LF, Bolam JP, Brown P, Magill PJ, 2008. Parkinsonian beta oscillations in the external globus pallidus and their relationship with subthalamic nucleus activity. J. Neurosci 28, 14245–14258. [PubMed: 19109506]

Mallet N, Micklem BR, Henny P, Brown MT, Williams C, Bolam JP, Nakamura KC, Magill PJ, 2012. Dichotomous organization of the external globus pallidus. Neuron 74, 1075–1086. [PubMed: 22726837]

Mao Z, He S, Mesnard C, Synowicki P, Zhang Y, Chung L, Wiesman AI, Wilson TW, Monaghan DT, 2020. NMDA receptors containing GluN2C and GluN2D subunits have opposing roles in modulating neuronal oscillations; potential mechanism for bidirectional feedback. Brain Res. 1727, 146571.

Mastro KJ, Bouchard RS, Holt HA, Gittis AH, 2014. Transgenic mouse lines subdivide external segment of the globus pallidus (GPe) neurons and reveal distinct GPe output pathways. J. Neurosci 34, 2087–2099. [PubMed: 24501350]

Mastro KJ, Zitelli KT, Willard AM, Leblanc KH, Kravitz AV, Gittis AH, 2017. Cell-specific pallidal intervention induces long-lasting motor recovery in dopamine-depleted mice. Nat. Neurosci 20, 815–823. [PubMed: 28481350]

Mullasseril P, Hansen KB, Vance KM, Ogden KK, Yuan H, Kurtkaya NL, Santangelo R, Orr AG, Le P, Vellano KM, Liotta DC, Traynelis SF, 2010. A subunit-selective potentiator of NR2C- and NR2D-containing NMDA receptors. Nat. Commun 1, 90. [PubMed: 20981015]

Rajput AH, Sitte HH, Rajput A, Fenton ME, Pifl C, Hornykiewicz O, 2008. Globus pallidus dopamine and Parkinson motor subtypes: clinical and brain biochemical correlation. Neurology 70, 1403–1410. [PubMed: 18172064]

Ravikrishnan A, Gandhi PJ, Shelkar GP, Liu J, Pavuluri R, Dravid SM, 2018. Region-specific expression of NMDA receptor GluN2C subunit in parvalbumin-positive neurons and astrocytes: analysis of GluN2C expression using a novel reporter model. Neuroscience 380, 49–62. [PubMed: 29559384]

Santangelo Freel RM, Ogden KK, Strong KL, Khatri A, Chepiga KM, Jensen HS, Traynelis SF, Liotta DC, 2013. Synthesis and structure activity relationship of tetrahydroisoquinoline-based potentiators of GluN2C and GluN2D containing N-methyl-D-aspartate receptors. J. Med. Chem 56, 5351–5381. [PubMed: 23627311]

Sheinin A, Shavit S, Benveniste M, 2001. Subunit specificity and mechanism of action of NMDA partial agonist D-cycloserine. Neuropharmacology 41, 151–158. [PubMed: 11489451]

Shelkar GP, Pavuluri R, Gandhi PJ, Ravikrishnan A, Gawande DY, Liu J, Stairs DJ, Ugale RR, Dravid SM, 2019. Differential effect of NMDA receptor GluN2C and GluN2D subunit ablation on behavior and channel blocker-induced schizophrenia phenotypes. Sci. Rep 9, 7572–019-43957–2.

Swanger SA, Vance KM, Pare JF, Sotty F, Fog K, Smith Y, Traynelis SF, 2015. NMDA receptors containing the GluN2D subunit control neuronal function in the subthalamic nucleus. J. Neurosci 35, 15971–15983. [PubMed: 26631477]

Traynelis SF, Wollmuth LP, McBain CJ, Menniti FS, Vance KM, Ogden KK, Hansen KB, Yuan H, Myers SJ, Dingledine R, 2010. Glutamate receptor ion channels: structure, regulation, and function. Pharmacol. Rev 62, 405–496. [PubMed: 20716669]

Vitek JL, Johnson LA, 2019. Understanding Parkinson's disease and deep brain stimulation: role of monkey models. Proc. Natl. Acad. Sci. U. S. A 116 (52), 26259–26265.

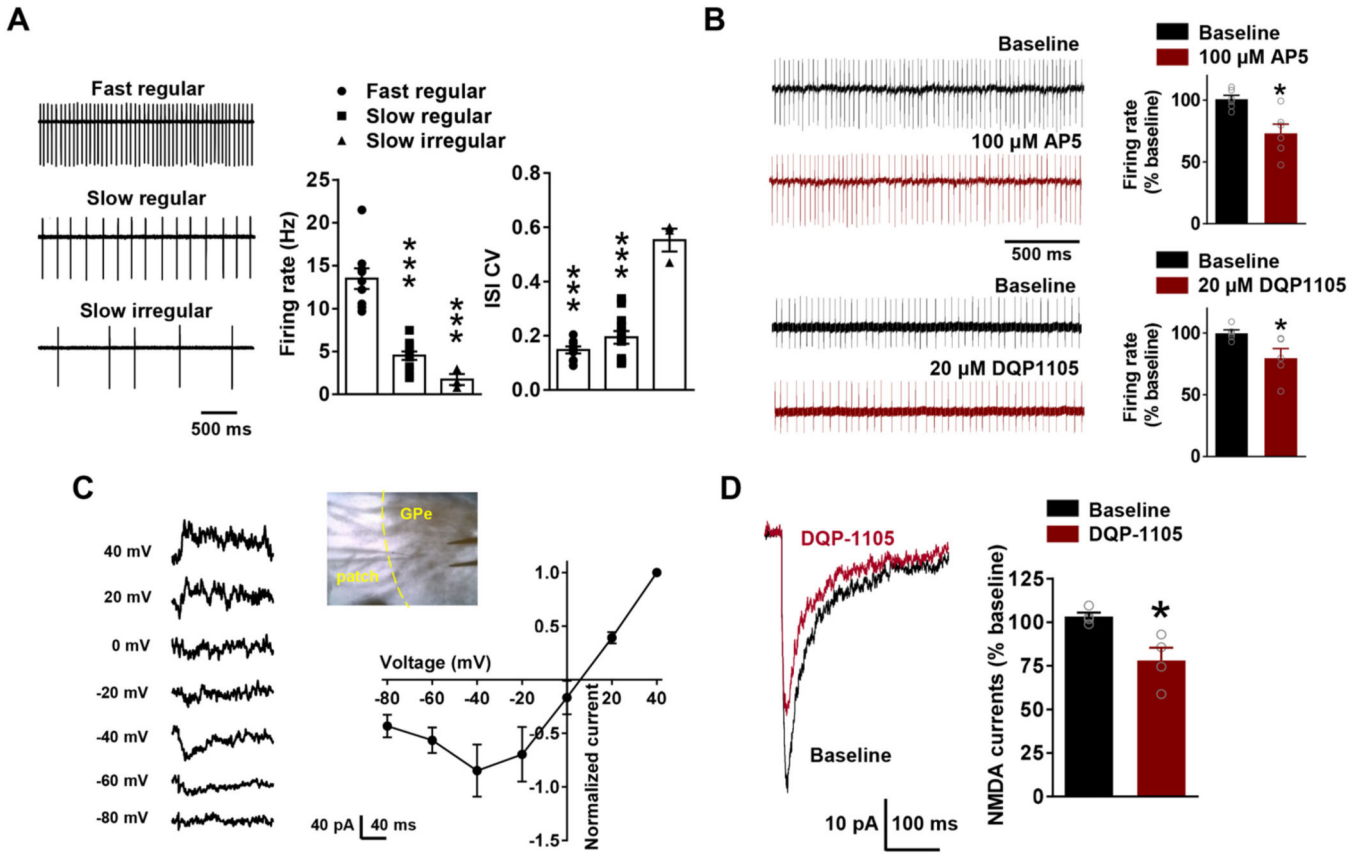

Fig. 1.

NMDA receptor currents from fast-regular spiking neurons are sensitive to GluN2C/2D inhibitor. **A.** Three cell types based on their firing pattern in cell-attached mode were identified. These included fast regular ($N = 9$), slow regular ($N = 12$) and slow irregular firing ($N = 3$) neurons. The firing rate and inter-spike interval (ISI) were significantly different in the three subpopulations of neurons in the GPe (***$p < 0.001$, firing rate F (2,21) = 39.90, ISI F (2, 21) = 42.08, one-way ANOVA with Tukey's multiple comparison). **B.** Effect of AP5 (100 μM) and DQP1105 (20 μM) in cell-attached recordings on firing of fast-spiking neurons. AP5 significantly reduced the firing of fast spiking neurons $N = 6$, *$p = 0.028$, paired *t*-test. A significant reduction was also observed with DQP1105. $N = 5$, *$p = 0.029$, paired *t*-test. **C.** Whole-cell voltage clamp recordings at holding potential of − 40 mV from GPe fast-spiking neurons was performed in the presence of 100 μM picrotoxin and 10 μM CNQX. The extracellular $MgCl_2$ was reduced to 0.2 mM. Stimulation of putative subthalamic neuron projections generated NMDA receptor currents in GPe neurons ($N = 8$). **D.** The evoked NMDA receptor currents were significantly inhibited by GluN2C/2D selective inhibitor DQP-1105 (20 μM), $N = 4$, *$p = 0.046$, paired t-test. All data are presented as mean ± SEM.

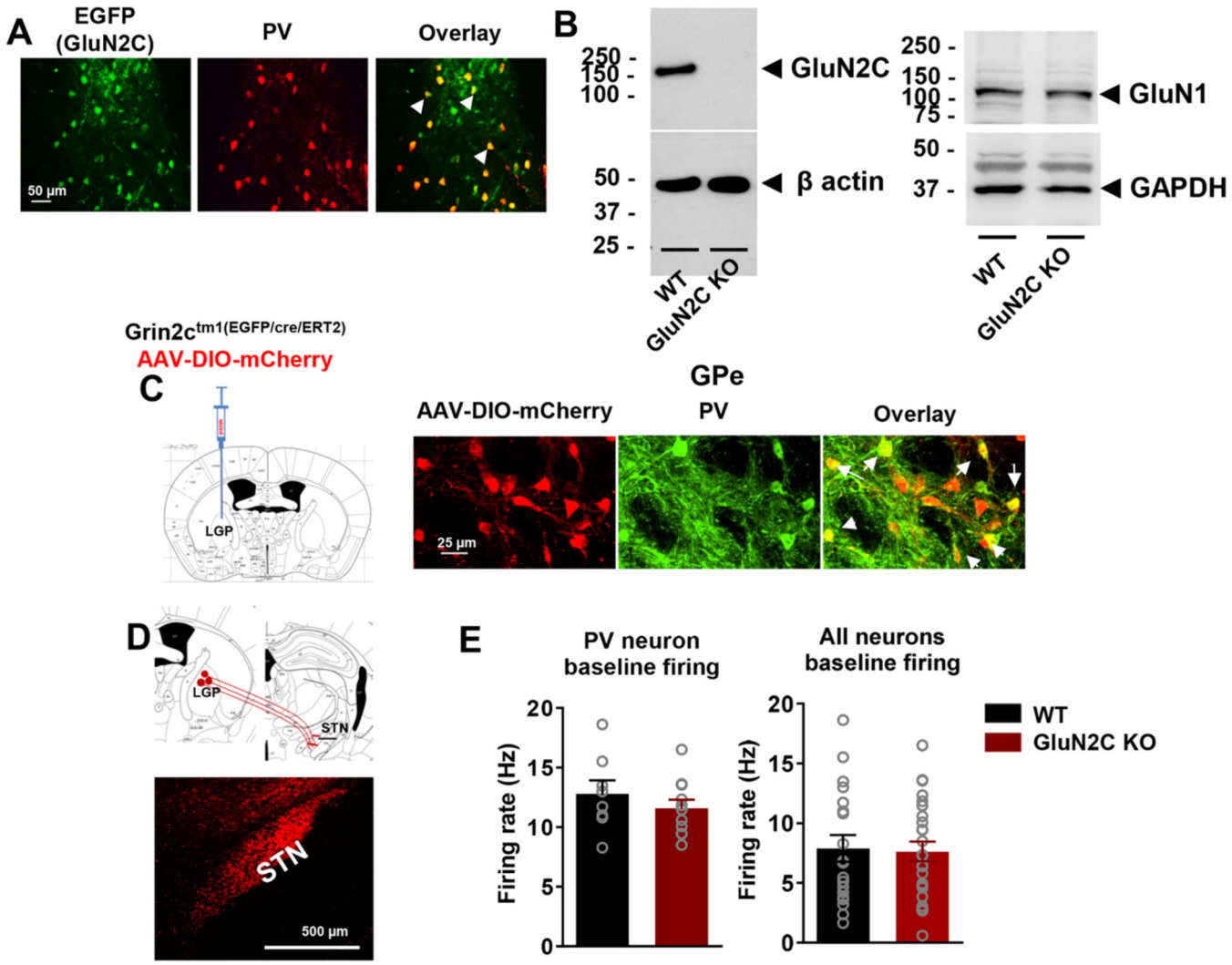

Fig. 2.

Expression of GluN2C subunit in the GPe PV neurons. **A.** Immunohistochemical analysis in Grin2C-EGFP-CreERT2 mouse model. Expression of EGFP in the Grin2C-reporter model was found to primarily co-localize with PV-positive neurons. Repeated 4 times. **B.** Western blot analysis of total protein lysate preparation from GPe of wildtype and GluN2C KO. Expression of GluN2C was observed in GPe in wildtype mice and lack in GluN2C KO preparation. Expression of obligatory GluN1 subunit was also found in GPe samples. **C.** Evaluation of cre-dependent reporter expression in Grin2C-EGFP-CreERT2. Mice were injected with AAV containing cre-dependent mCherry (AAV-DIO-mCherry) followed by tamoxifen induction. Immunohistochemistry was performed for PV. Reporter mCherry expression was observed in the GPe which colocalized with PV. **D.** Reporter mCherry labeled projections were found in the subthalamic nuclei. **E.** Firing rate of fast-spiking and non-fast-spiking neurons in the GPe was examined in wildtype and GluN2C KO mice. No difference was observed in firing rate in GPe fast-spiking neurons was observed in GluN2C KO mice (N = 8 WT, 11 GluN2C KO). No difference in the overall firing rate of all the recorded neurons was found in GluN2C KO (*N* = 19 WT, 25 GluN2C KO).

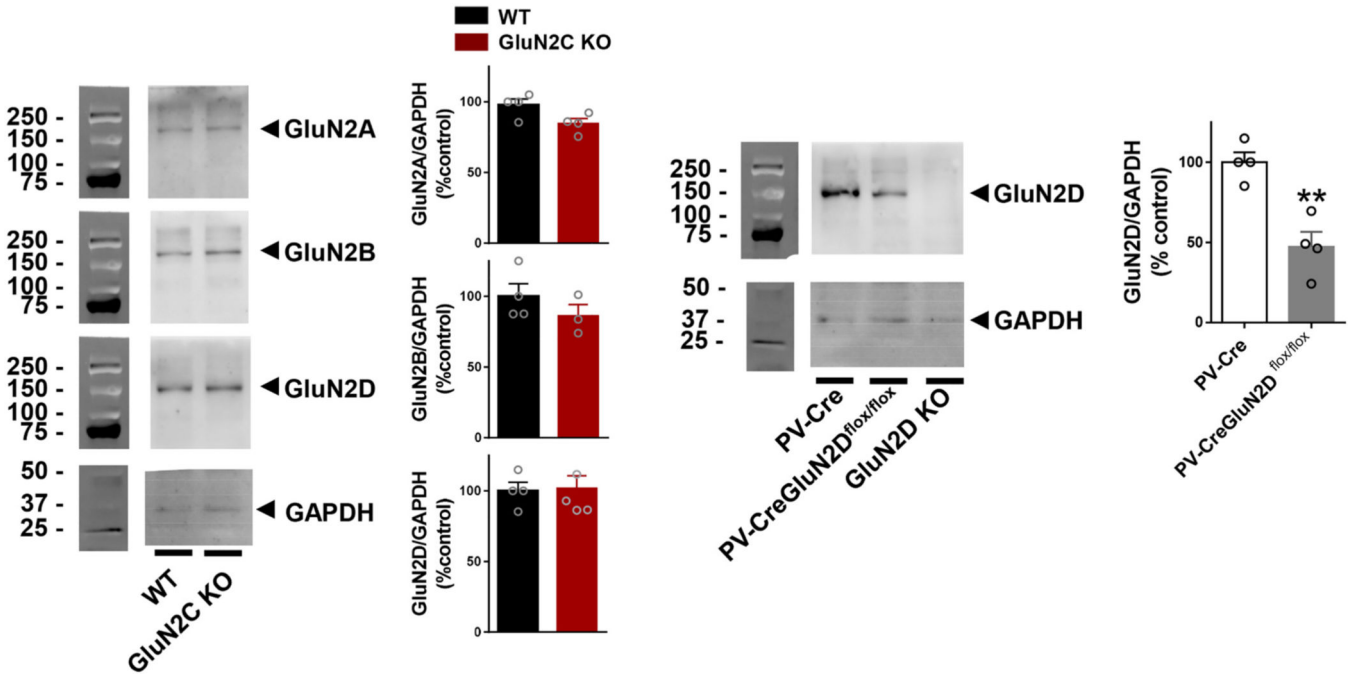

Fig. 3.

Effect of GluN2C deletion on expression of other NMDA receptor subunits in the GPe. **A.** Analysis of synaptoneurosome preparation for expression of GluN2A, GluN2B and GluN2D subunits from WT and GluN2C KO. No significant change in expression was observed in any of the GluN2 subunits (N = 3–5). **B.** Analysis of GluN2D expression in PV neurons in GPe. Conditional strategy for ablation of GluN2D from PV neurons. A significant reduction in the expression of GluN2D was observed in the PV-CreGluN2D$^{flox/flox}$ mice suggesting expression of GluN2D subunit in the PV neurons in the GPe. N = 4, *p = 0.0031, unpaired t-test.

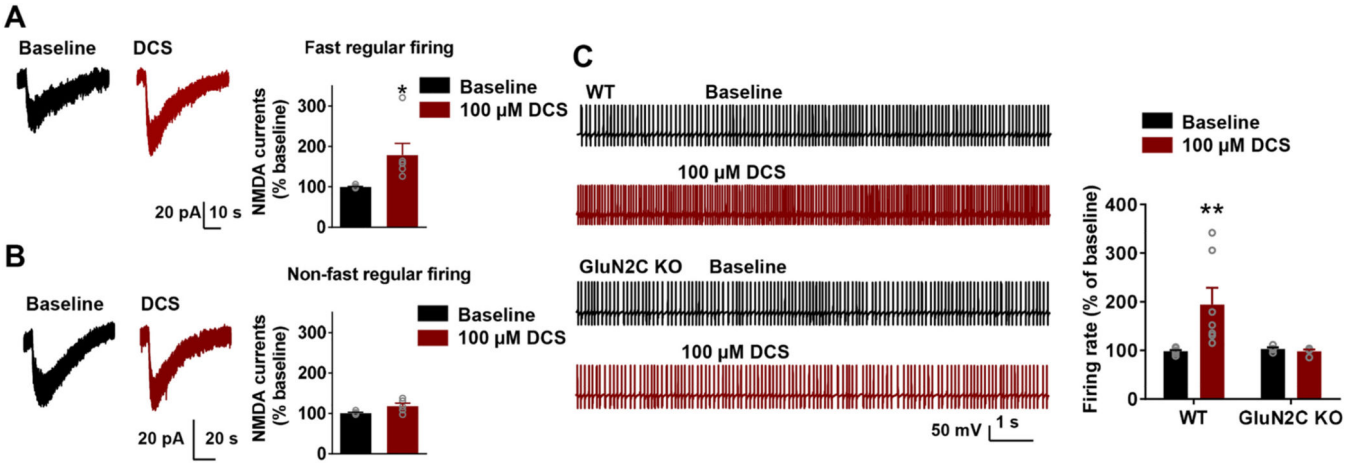

Fig. 4.

Fast-spiking neurons in the GPe are modulated by facilitation of GluN2C-containing receptors. **A.** Whole-cell voltage clamp recordings from GPe neurons at holding potential of − 40 mV in the presence of 100 μM picrotoxin and 10 μM CNQX. Effect of D-cycloserine (DCS) on NMDA receptor currents induced by puff application of 1 mM NMDA was examined in both fast-spiking and non-fast-spiking neurons. A significant increase in current amplitude was observed upon application of DCS in fast-spiking neurons. Baseline 99.58 ± 1.42% vs. 100 μM DCS 178.7 ± 28.95%, $N = 6$, $*p = 0.0443$, Paired t-test. Slight but non-significant increase in the currents in non-fast spiking neurons. Baseline 100.8 ± 2.0% vs. 100 μM DCS 118.2 ± 7.3%, N = 5, $p = 0.0648$, Paired t-test. **B.** Spontaneous firing recordings were obtained in whole-cell mode from fast-spiking GPe neurons from brain slices from wildtype and GluN2C KO mice. DCS increased the spontaneous firing of fast-spiking neurons in the GPe from wildtype but not in GluN2C KO. $N = 7$ WT, 4 GluN2C KO, Two-way ANOVA showed a significant interaction effect $F(1,18) = 4.629$, $p = 0.0453$. Bonferroni's post-hoc test $**p = 0.007$.

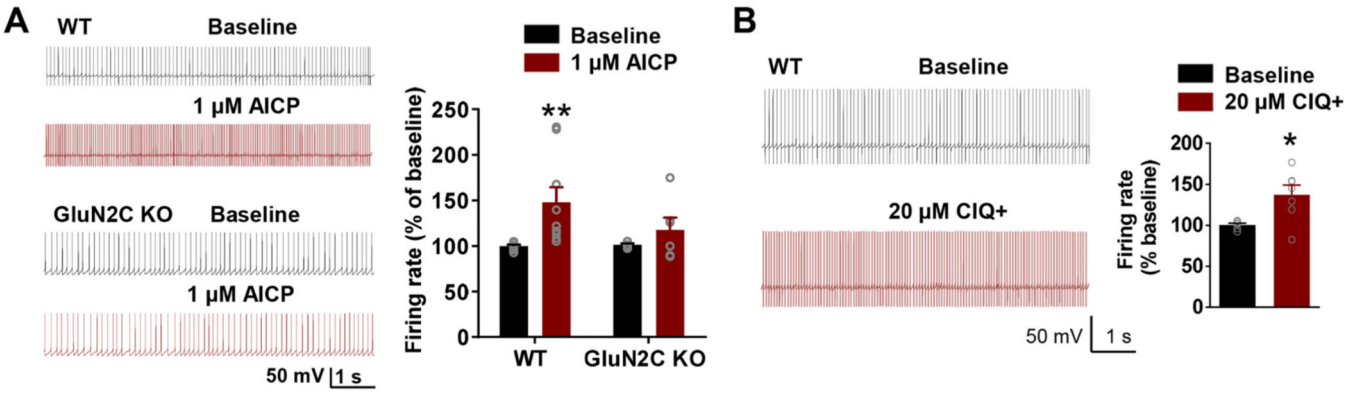

Fig. 5.

Novel glycine-site agonist AICP and GluN2C/2D positive allosteric modulator +CIQ increases firing of GPe fast-spiking neurons. **A.** In whole-cell the firing of GPe neurons was assessed and the effect of bath application of 1 μM AICP was evaluated. Increase in the firing rate was observed in wildtype but not in GluN2C KO. $N = 9$ WT, 6 GluN2C KO, Two-way ANOVA showed a significant drug effect $F(1,26) = 7.563$, $p = 0.0107$. Bonferroni's post-hoc test $^{**}p = 0.0065$. **B.** Effect of a positive allosteric modulator for GluN2C/2D-containing receptors (+)CIQ on GPe neuron firing. Bath application of 20 μM (+)CIQ increased the firing of fast-spiking neurons. N = 7, $^{*}p = 0.0244$, paired t-test.

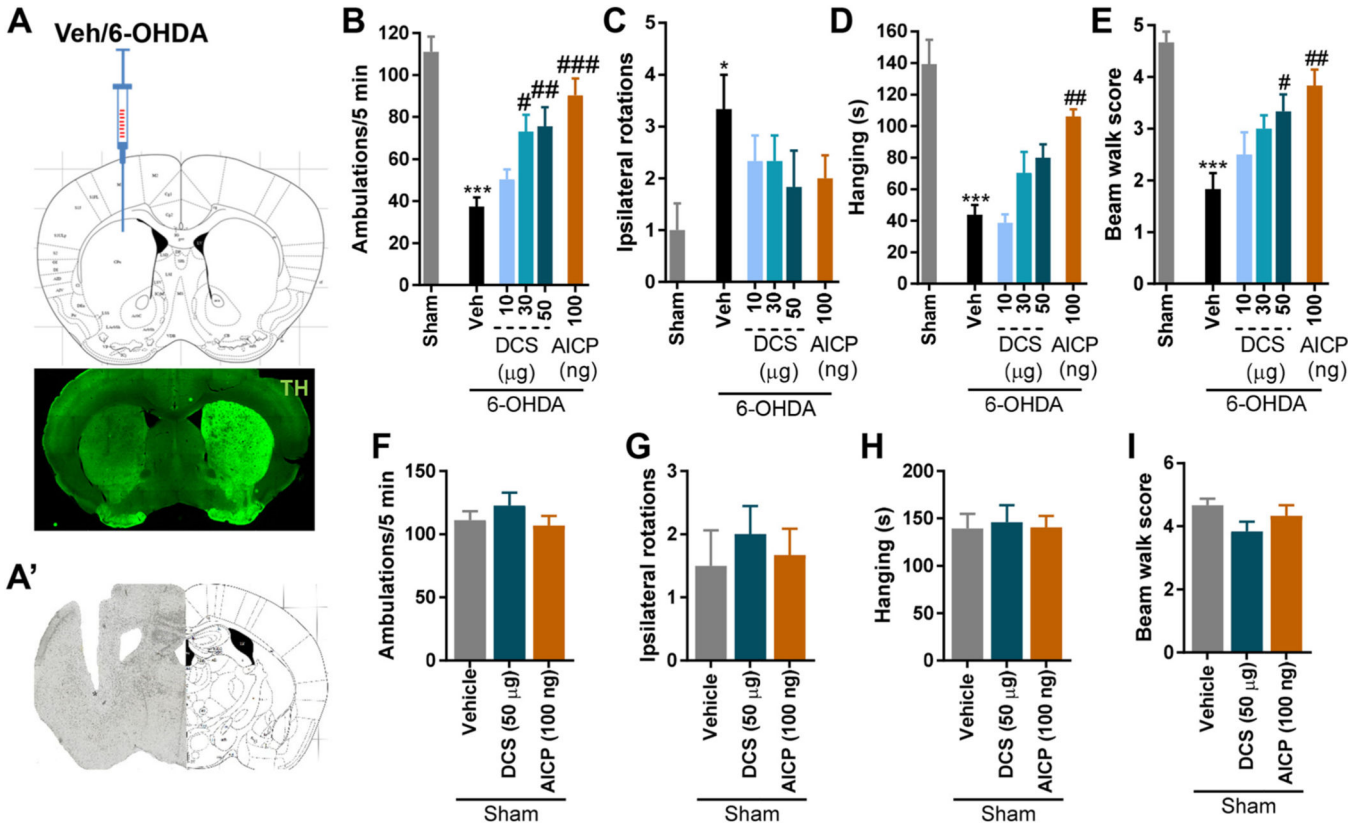

Fig. 6.

Facilitation of GluN2C-containing receptors in GPe by D-cycloserine (DCS) and AICP improve motor function in a 6-OHDA-induced mouse model of PD. **A.** Showing site of 6-OHDA injection and assessment of dopaminergic lesions by TH-immunostaining. **A'.** Verification of cannula placement in GPe. **B.** In the open field test, DCS (30 and 50 μg) and AICP significantly improved locomotor activity (N = 6/ group; One-way ANOVA with Bonferroni's post-hoc test [F (5, 30) = 13.9, $P < 0.0001$]). ***$P < 0.0001$ vs Sham, $^{\#}P = 0.01$, $^{\#\#}P = 0.009$, $^{\#\#\#}P = 0.0002$ vs 6-OHDA. **C.** No significant reduction in ipsilateral rotations by DCS and AICP (N = 6/ group; One-way ANOVA with Bonferroni's post-hoc test [F (5, 30) = 1.845, $P = 0.134$]). **D.** AICP significantly improved latency to fall in the wire hanging test (N = 6/ group; One-way ANOVA with Bonferroni's post-hoc test [F (5, 30) = 15.31, $P < 0.0001$]). ***$P < 0.0001$ vs Sham, $^{\#\#}P = 0.001$ vs 6-OHDA. **E.** In the beam walk test, DCS (50 μg) and AICP significantly improved beam walk score in 6-OHDA injected mice (N = 6/ group; One-way ANOVA with Bonferroni's post-hoc test [F (5, 30) = 10.03, $P < 0.0001$]). ***$P < 0.0001$ vs Sham, $^{\#}P = 0.03$, $^{\#\#}P = 0.001$ vs 6-OHDA). No significant differences in locomotor activity (**F**), ipsilateral rotations (**G**), latency to fall in the wire hanging test (**H**), and beam walk score (**I**) were observed in sham animals following DCS or AICP treatment (N = 6/group, $P > 0.05$).